Nonlinear parametric simulation by proper generalized decomposition on the example of a synchronous machine

Fabian Müller, Paul Baumanns, Martin Marco Nell and Kay Hameyer
Institute of Electrical Machines, RWTH Aachen University, Aachen, Germany

Received 8 November 2021
Revised 30 April 2022
Accepted 6 June 2022

Abstract

Purpose – The accurate simulation of electrical machines involves a large number of degrees of freedom. Particularly, if additional parameters such as remanence variations or different operating points have to be analyzed, the computational effort increases fast, known as the "curse of dimensionality." The purpose of this study is to cope with this effort with the parametric proper generalized decomposition (PGD) as a model order reduction (MOR) technique. It is combined with the discrete empirical interpolation method (DEIM) and adapted to study characteristic electrical machine parameters.

Design/methodology/approach – The PGD is an *a priori* MOR technique. The technique is adapted to incorporate several additional parameters, such as the current excitation or permanent magnet remanence, to overcome the increasing computational effort of parametric studies. Further, it is combined with the DEIM to approximate the nonlinearity of the flux guiding material.

Findings – The parametric version of the PGD in combination with the DEIM is a suitable numerical approach to reduce computational effort of parametric studies, while considering nonlinear materials. The computational reduction is related to the influence of the different parameter variations on the field and on the number of parameters.

Originality/value – The extension of the PGD by several parameters associated with parametric studies of electrical machines enables to cope with the "curse of dimensionality." The parametric PGD and the standard PGD–DEIM have been individually used to study different problems. The combination of both techniques, the parametric PGD and the DEIM, for nonlinear parametric studies of electrical machines represents the scientific contribution of this research.

Keywords Model order reduction, Proper generalized decomposition, Discrete empirical interpolation method, Finite element method, Synchronous machine, Electrical machine, Magnetic nonlinearity

Paper type Research paper

1. Introduction

The reduction of computational effort related to the numerical simulation of electromagnetic machines is a topic of increasing relevance. In the design stage, many parameter combinations have to be analyzed; on the one hand, different characteristic operating points have to be studied, whereas on the other hand, design parameters such as the remanence of the permanent magnets are of interest. In combination with the degrees of freedom (DOF)

This work was supported by the German Research Foundation (DFG) within the research project number 347941356 "Numerical Analysis of Electromagnetic Fields by Proper Generalized Decomposition in Electrical Machines."

COMPEL - The international journal for computation and mathematics in electrical and electronic engineering
Vol. 41 No. 4, 2022
pp. 1171-1180

0332-1649
DOI 10.1108/COMPEL-11-2021-0431

resulting from the spatial discretization of the finite element method (FEM), the computational effort increases quickly associated with the parameter variations. Model order reduction (MOR) techniques decrease the DOF to cope with this problem, by using approximations of the solution in a reduced subspace (Chaturantabut and Sorensen, 2010; Chinesta *et al.*, 2013; Henneron and Clénet, 2016a, 2016b; Krimm *et al.*, 2019; Müller *et al.*, 2020a, 2020b). The modeling and analysis of electrical machines in the FEM can be distinguished into a combination of different problem families. The nonlinear ferromagnetic material requires appropriate algorithms to handle the nonlinear problem. Furthermore, the movement-related problem deals with the motion of the rotor. Lastly, the parametric problem because of the above-mentioned variations results in large DOF. The proper generalized decomposition (PGD) is particularly suited for the analysis of electrical machines, because each parameter of interest can be introduced into the reduced framework. In Montier *et al.* (2016), a rotating electrical machine was linearly modeled with varying material parameters. Another linear parametric problem of an electric machine is presented in Sancarlos *et al.* (2021). However, it is limited by a structured finite element grid. A nonlinear transformer is simulated in Henneron and Clénet(2016a) with the PGD and a method to reduce the computational effort related to the evaluation of the nonlinear material by using the discrete empirical interpolation method (DEIM) is shown. Although the parametric PGD (Sancarlos *et al.*, 2021) and the PGD–DEIM (Henneron and Clénet, 2016a) have been used individually to simulate different applications, a combination of both to simulate electrical machines is not yet made. In this paper, a permanent magnet synchronous machine (PMSM) with a parametric excitation is simulated by a parametric PGD in conjunction with the DEIM. The nonlinear material is considered and furthermore, no restriction to structured meshes is necessary. The operating points in terms of current excitation of electrical machines are commonly denoted in the dq-plane. To enable the PGD to approximate the machine behavior in different operating points and for different permanent magnet materials, the method is extended by parameters for the permanent magnet remanence B_r, the current amplitude $\hat{\mathrm{I}}$ and current angle ϕ.

2. Fundamentals

2.1 Synchronous machine theory

In the operation of PMSM, the excitation field is superposed with the armature field given by the current in the stator windings. Although the current is usually a three-phase current, it is practically more useful to transform the currents into the dq-plane. The direct axis is directed along the magnet flux and the quadrature axis is placed between two magnetic poles. The phase advance ϑ is given by the angle of the synchronous generated internal voltage to the stator flux. The definitions are depicted in Figure 1. The total number of simulations to characterize the operating points of interest is then defined by

$$N_{Sim} = N_{Rotor} \cdot \hat{\mathrm{I}} \cdot \phi \cdot B_\mathrm{r}. \tag{1}$$

N_Rotor denotes the number of modeled rotor positions.

2.2 Finite element method

Because of the complicated geometry of electrical machines, the FEM with the magnetic vector potential is used. The electrical machine is considered as a bounded domain Ω, holding a coupling interface Γ between rotor and stator airgap. The movement is realized by using a sliding interface technique (Lange *et al.*, 2010) to model arbitrary rotor position and ensuring continuity along the air gap. Because of the nonlinear behavior of electrical steel

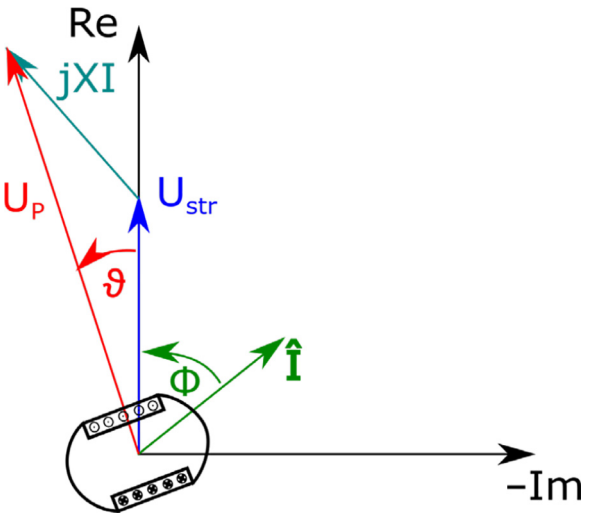

Figure 1.
Current and angle definitions

sheets, it is necessary to use a nonlinear iteration scheme, such as the fixed-point method (Saitz, 1999):

$$\nabla \times \left(\nu_{\mathrm{fp}} \nabla \times \boldsymbol{A}(\boldsymbol{x}, p_1, \ldots, p_n) = \boldsymbol{J} + \nabla \times \nu \boldsymbol{B}_{\mathrm{r}} - \nabla \times \left(\boldsymbol{H}_{\mathrm{fp}}(\boldsymbol{x}, p_1, \ldots, p_n)\right), \right. \tag{2}$$

where $\boldsymbol{A}$ is the magnetic vector potential, $\boldsymbol{J}$ is the current density in the coils and $\boldsymbol{x}$ denotes the space. ν_{fp} is the fixed-point reluctivity and permanent magnets are considered by $\boldsymbol{B}_{\mathrm{r}}$. The nonlinearity is considered by the virtual magnetization vector $\boldsymbol{H}_{\mathrm{fp}}$.

3. Model order reduction by proper generalized decomposition

MOR techniques are based on the approach that the unknown potentials can be decomposed into products of functions that depend on only one variable such as space or time (equation 2) (Nouy, 2010; Henneron and Clénet, 2016a, 2017; Müller *et al.*, 2020a, 2020b). By approximating the unknown solution only in a subspace, the DOFs and the computational effort can be reduced.

$$\boldsymbol{U}(\boldsymbol{x}, p_1, \ldots, p_n) \approx \sum_{i=1}^{\mathrm{m}} \boldsymbol{R}_i(\boldsymbol{x}) \cdot F_{i,1}(p_1) \cdot \ldots \cdot F_{i,n}(p_n) \tag{3}$$

In equation (3), the vector $\boldsymbol{U}$ represents the magnetic vector potential $\boldsymbol{A}$ with a finite number of terms m. These terms are also commonly called modes. These modes decompose the parametric solution space into independent coordinates. In terms of parametric simulation of electrical machines, the introduced coordinates are the space $\boldsymbol{x}$, which is represented by the space modes $\boldsymbol{R}_i$. The current amplitude and angle, as well as the magnet remanence, are considered by $F_{i,1}$–$F_{i,3}$. Other variables, that do not change the mesh, can be introduced too (Montier *et al.*, 2016).

Depending on the problem dimension, the spatial component $R(x)$ is modeled in the edge or nodal element space, whereas the other functions are approximated in $\mathbb{R}$. To further

minimize the computational effort associated with the nonlinearity, a second technique, the DEIM, is used (Chaturantabut and Sorensen, 2010). The DEIM approximates the nonlinear behavior by evaluating the nonlinear term only on a subset of elements connected to certain nodes. Therefore, the nonlinearity in distinct steps is evaluated and decomposed by a singular value decomposition, resulting in an orthogonal basis spanning a subspace of the nonlinear space. Consecutively, it is analyzed by a greedy algorithm to extract the most important indices minimizing a residual (Chaturantabut and Sorensen, 2010; Henneron and Clénet, 2016a; Müller *et al.*, 2021).

It shall be mentioned that an untruncated DEIM basis can lead to instabilities or inaccuracies in some cases (Hasan *et al.*, 2018). To cope with this behavior, the basis is truncated after the most information content is sought into the DEIM approximation (Müller *et al.*, 2021).

3.1 Computation of space mode

Assuming modes up to $m-1$ are known, the spatial component can be computed by equation (4), which is achieved by introducing the approach (equation 2) into the nonlinear magnetostatic formulation (equation 1). The element shape functions are reformulated into

$$\begin{aligned}\alpha = \; & \boldsymbol{R}_m^{'}(\boldsymbol{x}) \cdot F_{m,\ 1}(p_1) \cdot \ldots \cdot F_{m,\ n}(p_n) + \boldsymbol{R}_m(\boldsymbol{x}) \cdot F_{m,\ 1}^{'}(p_1) \cdot \ldots \cdot F_{m,\ n}(p_n) + \ldots \\ & + \boldsymbol{R}_m(\boldsymbol{x}) \cdot F_{m,\ 1}(p_1) \cdot \ldots \cdot F_{m,\ n}^{'}(p_n).\end{aligned} \tag{4}$$

The nonlinear term depends on the approximation of the solution $\boldsymbol{A}(x, p_1, \ldots, p_n)$ and to cope with the related computational effort of evaluating $\boldsymbol{H}_{\mathrm{fp}}$ in the reference system, the DEIM is used (Henneron and Clénet, 2016a). Using equations (3) and (4) in equation (1) results in equation (5). All terms except for the last one on the right-hand side (RHS) are separated by parameters, which allows a fast evaluation. However, the last term on the RHS depends on the solution in the reference system to assess $\boldsymbol{H}_{\mathrm{fp}}$ and states the largest computational effort. Using the DEIM significantly reduces the effort of this term by only evaluating the nonlinearity in selected elements and projecting the nonlinearity onto the complete system (Chaturantabut and Sorensen, 2010; Henneron and Clénet, 2016a; Müller *et al.*, 2021).

$$\begin{aligned}&\sum_{i=1}^{m} \int_{p_1} F_{i,1}(p_1) F_{m,1}(p_1) \mathrm{d}p_1 \cdot \ldots \quad \cdot \int_{p_n} F_{i,n}(p_n) F_{m,n}(p_n) \mathrm{d}p_n \int_{\Omega} \nu_{\mathrm{fp}} \nabla \times \boldsymbol{R}_i(\boldsymbol{x}) \nabla \times \boldsymbol{R}_m^{'}(\boldsymbol{x}) \mathrm{d}\Omega \\ &= \int_{p_1} J_{i,1}(p_1) F_{m,1}(p_1) \mathrm{d}p_1 \cdot \cdot \int_{p_n} J_{i,\mathrm{n}}(p_n) F_{\mathrm{n,m}}(p_n) \mathrm{d}p_{\mathrm{n}} \int_{\Omega} \boldsymbol{J}(\boldsymbol{x}) \boldsymbol{R}_m^{'}(\boldsymbol{x}) \ \mathrm{d}\Omega - \int_{p_1} F_{\mathrm{m},1}(p_1) \cdot \ldots \\ &\cdot \int_{p_n} F_{\mathrm{m,n}}(p_n) \mathrm{d}p_n \int_{\Omega} \boldsymbol{H}_{\mathrm{fp}}\left(\boldsymbol{A}(\boldsymbol{x}, p_1, \ldots, p_n)\right) \nabla \times \boldsymbol{R}_m^{'}(\boldsymbol{x}) \mathrm{d}\ \Omega \mathrm{d}p_{\mathrm{n}} \cdot \ldots \mathrm{d}p_1\end{aligned} \tag{5}$$

3.2 Computation of other parameter modes

After the space mode is computed, the next steps consist of computation of the other parameter functions. As an example, the parameter function for p_1 shall be computed,

nevertheless the procedure is similar for the other scalar parameters. Again, assuming all other parameters are known, the form function is expressed as

$$\alpha = \; R(x) \cdot F'_{m,1}(p_1) \cdot \ldots \cdot F_{m,n}(p_n) \tag{6}$$

Substitution of equation (6) into equation (2) leads to

$$\begin{aligned}
&\sum_{i=1}^{m} \int_{p_1} F_{i,1}(p_1) F'_{m,1}(p_1) \mathrm{d}p_1 \cdot \ldots \cdot \int_{p_n} F_{i,n}(p_n) F_{m,n}(p_n) \mathrm{d}p_n \int_{\Omega} \nu_{\mathrm{fp}} \nabla \times \boldsymbol{R}_i(\boldsymbol{x}) \nabla \times \boldsymbol{R}_m(\boldsymbol{x}) \mathrm{d}\,\Omega \\
&= \int_{p_1} J_1(p_1) F'_{m,1}(p_1) \mathrm{d}p_1 \cdot \ldots \cdot \int_{p_n} J_n(p_n) F_{n,m}(p_n) \mathrm{d}p_n \int_{\Omega} \boldsymbol{J}(\boldsymbol{x}) \boldsymbol{R}_m(\boldsymbol{x}) \; \mathrm{d}\,\Omega - \int_{p_1} F'_{m,1}(p_1) \cdot \ldots \\
&\cdot \int_{p_n} F_{\mathrm{m,n}}(p_{\mathrm{n}}) \int_{\Omega} \boldsymbol{H_{fp}}\big(\boldsymbol{A}(\boldsymbol{x}, p_1, \ldots, p_n)\big) \nabla \times \boldsymbol{R}_m(\boldsymbol{x}) \mathrm{d}\,\Omega \mathrm{d}p_n \cdot \ldots \mathrm{d}p_1.
\end{aligned} \tag{7}$$

Equation (7) can now be reformulated into a strong formulation leading to a linear equation (8)

$$A_{p_1} F_{1,m}(p_1) = C_{p_1} J_1(p_1) - L(p_1) - M_{\mathrm{fp}}(p_1), \tag{8}$$

with the coefficients in equations (9)–(12) given by integration on the finite element mesh:

$$A_{p_1} = \int_{\Omega} \nu_{\mathrm{fp}} \nabla \times \boldsymbol{R}_m(\boldsymbol{x}) \nabla \times \boldsymbol{R}_m(\boldsymbol{x}) \mathrm{d}\,\Omega \cdot \prod_{j=2}^{n} \int_{p_j} F_{j,m}(p_j) F_{j,m}(p_j) \mathrm{d}p_j \tag{9}$$

$$C_{p_1} = \int_{\Omega} \boldsymbol{J}(\boldsymbol{x}) \boldsymbol{R}_m(\boldsymbol{x}) \mathrm{d}\,\Omega \cdot \prod_{j=2}^{n} \int_{p_j} J_j(p_j) F_{j,m}(p_j) \mathrm{d}p_j, \tag{10}$$

$$L(p_1) = \sum_{i=1}^{m-1} F_{i,1}(p_1) \int_{\Omega} \nu_{\mathrm{fp}} \nabla \times \boldsymbol{R}_i(\boldsymbol{x}) \nabla \times \boldsymbol{R}_m(\boldsymbol{x}) d\,\Omega \cdot \prod_{j=1}^{n} \int_{p_j} F_{i,j}(p_j) F_{m,j}(p_j) dp_j, \tag{11}$$

$$M_{\mathrm{fp}}(p_1) = \int_{p_2} F_2(p_2) \mathrm{d}p_2 \cdot \ldots \cdot \int_{\Omega} \boldsymbol{H_{fp}}\big(\boldsymbol{A}(\boldsymbol{x}, p_1, \ldots, p_n)\big) \cdot \nabla \times \boldsymbol{R_m}(\boldsymbol{x}) \mathrm{d}\,\Omega \mathrm{d}p_{\mathrm{n}} \cdot \ldots \mathrm{d}p_2 \tag{12}$$

3.3 Post processing

In standard finite element simulations, the relative position of the rotor to the stator is considered in the solving process by using interface conditions. In Montier *et al.* (2016), the rotational movement is used as an additional parameter, but the presented approach uses

one PGD model for each rotor position as in Sancarlos *et al.* (2021) and interpolating in between. This approach has an advantage, because it is also applicable with other formulations and three-dimensional problems. However, the drawback is that several PGD models have to be computed. In combination with introducing the current amplitude and angle, it is possible to extract rotational machine characteristics in the post processing stage.

4. Application

The PGD is applied to an exemplary synchronous machine with surface mounted permanent magnets, shown in Figure 2. The machine has a nominal speed of 3,000 rpm and a rated torque of 3 Nm at a current of 7 A. Different simulations, which occur in the design and analysis of electrical machines, will be given. In a first step, the remanence of the machine will vary as a design variable. In a second step, the remanence is varied and the current phasor is modified both in angle and amplitude. Different scenarios are studied, namely, locked rotor and different operating points in the *dq*-plane. The example concludes with an analysis of the influence of the number of parameters on the convergence and the computational effort.

4.1 Remanence as a design parameter

In the design of PMSM, different hard magnetic materials may be considered or derivations associated with the nonideal manufacturing shall be studied. By introducing the magnet remanence as a variable parameter into the PGD, an easy and fast analysis of the magnets effect on the machine behavior is given. The remanence is varied in five steps from 0.8 to 1.2 T and the electric angle is modified with a step width of five degree, leading to a total number of 360 parameter combinations.

The absolute residual for a distinct parameter combination i is calculated by equation (13) and the average error of all n parameter combinations is given by equation (14).

$$\epsilon_{\text{Abs}} = \frac{||B_i - \text{M}X_{PGD,\ i}||}{||B_i||} \tag{13}$$

$$\epsilon_{\text{Abs,}\quad\text{Ave}} = \frac{\sum_{i=1}^{n} \epsilon_{\text{Abs}}}{n} \tag{14}$$

In Figure 3(a), the averaged absolute residual versus the number of modes show that with a small number of modes, it is possible to achieve an accurate representation of the machine.

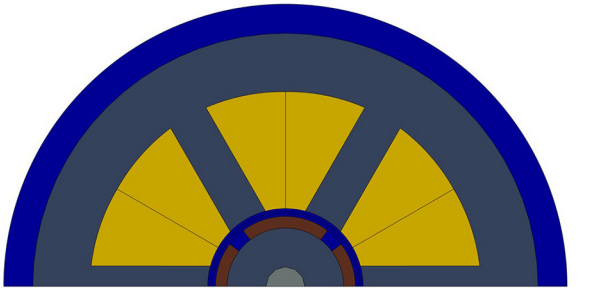

Figure 2.
Cross section of the simulated PMSM

The error versus electrical angle, shown in Figure 3(b), depicts that the error in each step is smaller than 1.5%. The smallest remanence exhibits the largest absolute errors. The torque for the lockstep simulation is given in Figure 3(c). The overall torque is well approximated yet a small deviation is noticeable, which slightly increases at lower remanence values, being in accordance with the absolute residual shown in Figure 3(b). The variation of the remanence changes the saturation of the material in the machine. Lowering the remanence below 1 T shows a greater influence on the overall material saturation compared to increasing the remanence over 1 T. Using several PGD models, one for each rotor position, enables the analysis of rotating machines. In Figure 3(d), the torque is given for different operating points; Point 1 is a no-load point (I_{dq} = [7, 0] A, B_r = 1.2 T), Point 2 depicts the rated torque (I_{dq} = [0, 7] A, B_r = 1.2 T) and Point 3 is an arbitrary working point at (I_{dq} = [2.82, −2.82] A, B_r = 1.2 T). The results indicate that the overall torque for different rotor positions is well approximate for the first two operating points. In the third operating point, an offset of 10% between reference and PGD solution is present, but the overall characteristic is similar. This offset results in an underestimated torque in this working point. While the first and second operating points have a similar current amplitude of 7 A, which saturates the material, the third has a smaller amplitude of 4 A. In this point, the influence of remanence variations on the field distribution is higher because of the nonlinear material characteristic. Although in the third operating point an offset is present, it can be concluded that the reduced model is accurate enough to approximate the torque characteristic of the machine in a first design step with only seven modes per angular position.

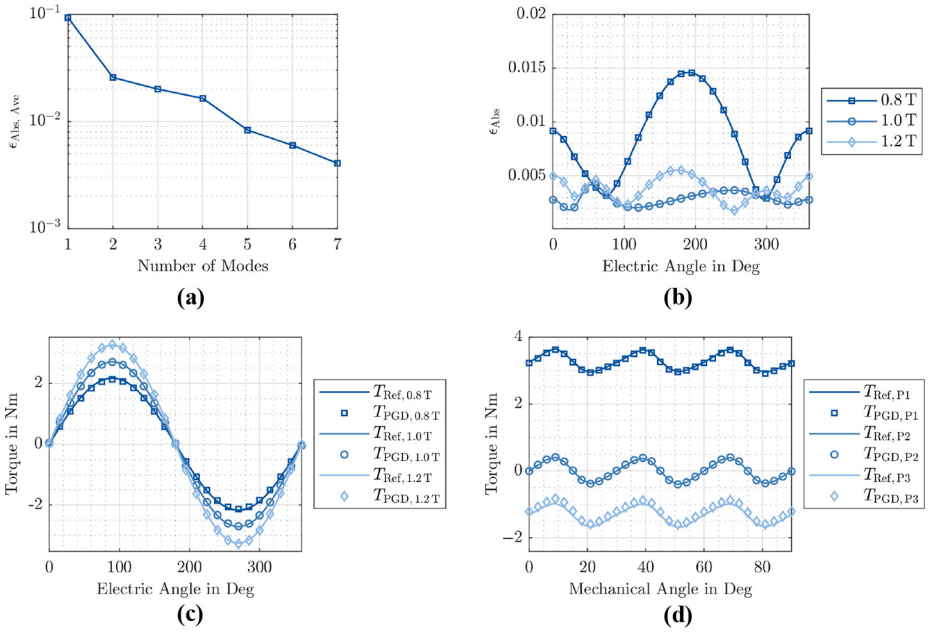

Figure 3. Absolute error and torque for simulations with different permanent magnet remanence values

Notes: (a) Average absolute residual versus number of modes; (b) absolute residual for different remanence values versus the electric angle; (c) torque for locked rotor configuration; (d) torque for different operating points

4.2 Current and remanence variation

After the influence of a remanence variation is studied, in the second case, the remanence, the current amplitude and the angle are varied, stating a larger influence on the saturation as well as on the flux density distribution in the machine. The amplitude interval $\hat{I} = [0, 7]$ A is equally divided into eight steps and the angle is treated similarly as in the previous case. The absolute residual, given in Figure 4(a), converges slightly slower in comparison to the previous simulation depicted in Figure 3(a). Therefore, nine modes have to be enriched to achieve an accuracy lower than 0.5%. From Figure 4(b), it can be concluded that the overall torque is close to the reference values. In contrast to the previous simulation, where the current amplitude is fixed, the deviations of the reduced model's torque and the reference solution behaves differently. In the previous study, the error between reduced torque and reference values is represented by a percentual offset, but in this study, the computed torque values are in some steps higher and others smaller than the reference, which is particularly present in operating point one and three. Further, operating point P3 shows a smaller average torque error. The overall torque deviations are smaller than for the previous study which may indicate that the remaining error of the PGD solution is not located near the air

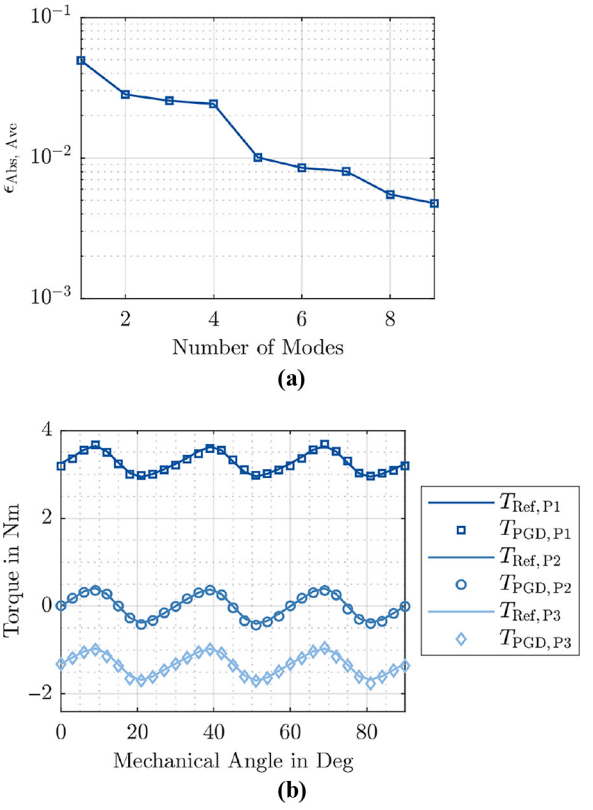

Figure 4.
Simulations varying current phasor and magnet remanence

Notes: (a) Average residual for a locked rotor configuration; (b) torque in different operating points

gap. The remaining inaccuracy may be justified by the many different saturations that are to be considered in the nonlinear problem, which contains four parameters in contrast to three of the previous studies. The reduced model, which contains the solution for 1,480 different parameter combinations, approximates the studied cases well with a small torque error.

4.3 Parameter influence

In the study, the number of modes necessary to reach a reasonable accuracy varies with the number of parameter combinations. On the one hand, the remanence variations between 0.8 and 1.2 T influence the air gap flux density, however, the main flux density distribution does not change significantly. On the other hand, the variations of the current amplitude between 0 and 7 A as well as the current angle have a large impact on the overall field distribution in the machine which leads to the higher number of modes necessary to achieve precise results. The ratio between the total amount of possible parameter combinations is not linearly proportional to the number of modes. While in the first study 360 combinations are given, the second one holds 2,880 parameter configurations; however, the number of associated modes is only seven for case one and nine for case two although the number of possible parameter combinations increased by a factor of eight. The computational effort for the first case was reduced by 41% and the second case by 57%. At this point it should be remarked that the IEM inhouse software is yet to be further optimized. In comparison to Sancarlos *et al.*(2021), the limitation to linear material and structured meshes is abolished. The simulations shown in this contribution are computed on a single core and do not exploit parallelization. This implies that faster computing cores reduces the computational time but not the computational effort in terms of operations. Therefore, it is conceivable that the subject of MOR in combination with faster central processing unit's (CPU's) and parallelization strategies is a further step toward real time simulations.

5. Conclusion

The PGD is used to simulate a PMSM with varying excitation parameters such as the remanence flux density of the PMSM and the current amplitude and angle. Different characteristic simulations are shown and discussed. The results highlight that the PGD produces accurate results both in global quantities such as the torque as well as in the mathematical residual dropping below 0.5% and is therefore in a technical relevant magnitude. The computational effort is reduced by the PGD and the machine behavior can be studied with reasonable accuracy. Future work will study the integration of the relative rotor position as a parameter to the PGD.

References

Chaturantabut, S. and Sorensen, D.C. (2010), "Nonlinear model reduction via discrete empirical interpolation", *SIAM Journal on Scientific Computing*, Vol. 32 No. 5, pp. 2737-2764.

Chinesta, F., Keuning, R. and Leygue, A. (2013), *The Proper Generalized Decomposition for Advanced Numerical Simulations: A Primer*, Springer Briefs, Berlin.

Hasan, M.R., Montier, L., Henneron, T. and Sabariego, R.V. (2018), "Stabilized reduced-order model of a non-linear Eddy current problem by a Gappy-POD approach", *IEEE Transactions on Magnetics*, Vol. 54 No. 12, pp. 1-8.

Henneron, T. and Clénet, S. (2016a), "Application of the PGD and DEIM to solve a 3-D non-linear magnetostatic problem coupled with the circuit equations", *IEEE Transactions on Magnetics*, Vol. 52 No. 3, pp. 1-4.

Henneron, T. and Clénet, S. (2016b), "Parametric analysis of magnetoharmonic problem based on proper generalized decomposition", *IEEE Conference on Electromagnetic Field Computation (CEFC)*, Miami, FL, p. 1.

Henneron, T. and Clénet, S. (2017), "Application of the proper generalized decomposition to solve magnetoelectric problem", *IEEE Transactions on Magnetics*, Vol. 54 No. 3, pp. 1-4.

Krimm, A., Casper, T., Schöps, S., De Gersem, H. and Chamoin, L. (2019), "Proper generalized decomposition of parameterized electrothermal problems discretized by the finite integration technique", *IEEE Transactions on Magnetics*, Vol. 55 No. 6, pp. 1-4.

Lange, E., Henrotte, F. and Hameyer, K. (2010), "A variational formulation for nonconforming sliding interfaces in finite element analysis of electric machines", *IEEE Transactions on Magnetics*, Vol. 46 No. 8, pp. 2755-2758.

Montier, L., Henneron, T., Clénet, S. and Goursaud, B. (2016), "Transient simulation of an electrical rotating machine achieved through model order reduction", *Advanced Modeling and Simulation in Engineering Sciences*, Vol. 3 No. 1, pp. 1-17.

Müller, F., Crampen, L., Henneron, T., Clénet, S. and Hameyer, K. (2020a), "Model order reduction techniques applied to magnetodynamic T-Ω-formulation", *Compel – The International Journal for Computation and Mathematics in Electrical and Electronic Engineering*, Vol. 39 No. 5, pp. 1057-1069.

Müller, F., Henneron, H., Clénet, S. and Hameyer, K. (2020b), "Error estimators for proper generalized decomposition in time-dependent electromagnetic field problems", *IEEE Transactions on Magnetics*, Vol. 56 No. 1, pp. 1-4.

Müller, F., Siokos, A., Kolb, J., Nell, M. and Hameyer, K. (2021), "Efficient estimation of electrical machine behavior by model order reduction", *IEEE Transactions on Magnetics*, Vol. 57 No. 6, pp. 1-4.

Nouy, A. (2010), "A priori model reduction through proper generalized decomposition for solving time-dependent partial differential equations", *Computer Methods in Applied Mechanics and Engineering*, Vol. 199 Nos 23/24, pp. 1603-1626.

Saitz, J. (1999), "Newton-Raphson method and fixed-point technique in finite element computation of magnetic field problems in media with hysteresis", *IEEE Transactions on Magnetics*, Vol. 35 No. 3, pp. 1398-1401.

Sancarlos, A., Ghnatios, C., Duval, J., Cueto, E. and Chinesta, F. (2021), "Fast computation of multi-parametric electromagnetic fields in synchronous machines by using PGD-based fully separated representations", *Energies*, Vol. 14 No. 5, p. 1454.

Corresponding author
Fabian Müller can be contacted at: fabian.mueller@iem.rwth-aachen.de